Supporting information for "Andreev interference in the surface accumulation layer of half-shell InAsSb/Al hybrid Nanowires"

Lukas Stampfer,[1] Damon J. Carrad,[1] Dags Olsteins,[1] Christian E. N. Petersen,[1] Sabbir A. Khan,[1,2] Peter Krogstrup,[1,2] and Thomas S. Jespersen[1,3,*]

[1] *Center for Quantum Devices, Niels Bohr Institute, University of Copenhagen, Universitetsparken 5, 2100 Copenhagen, Denmark.*
[2] *Microsoft Quantum Materials Lab Copenhagen, 2800 Lyngby, Denmark*
[3] *Department of Energy Conversion and Storage, Technical University of Denmark, Fysikvej, Building 310, 2800 Kgs. Lyngby*

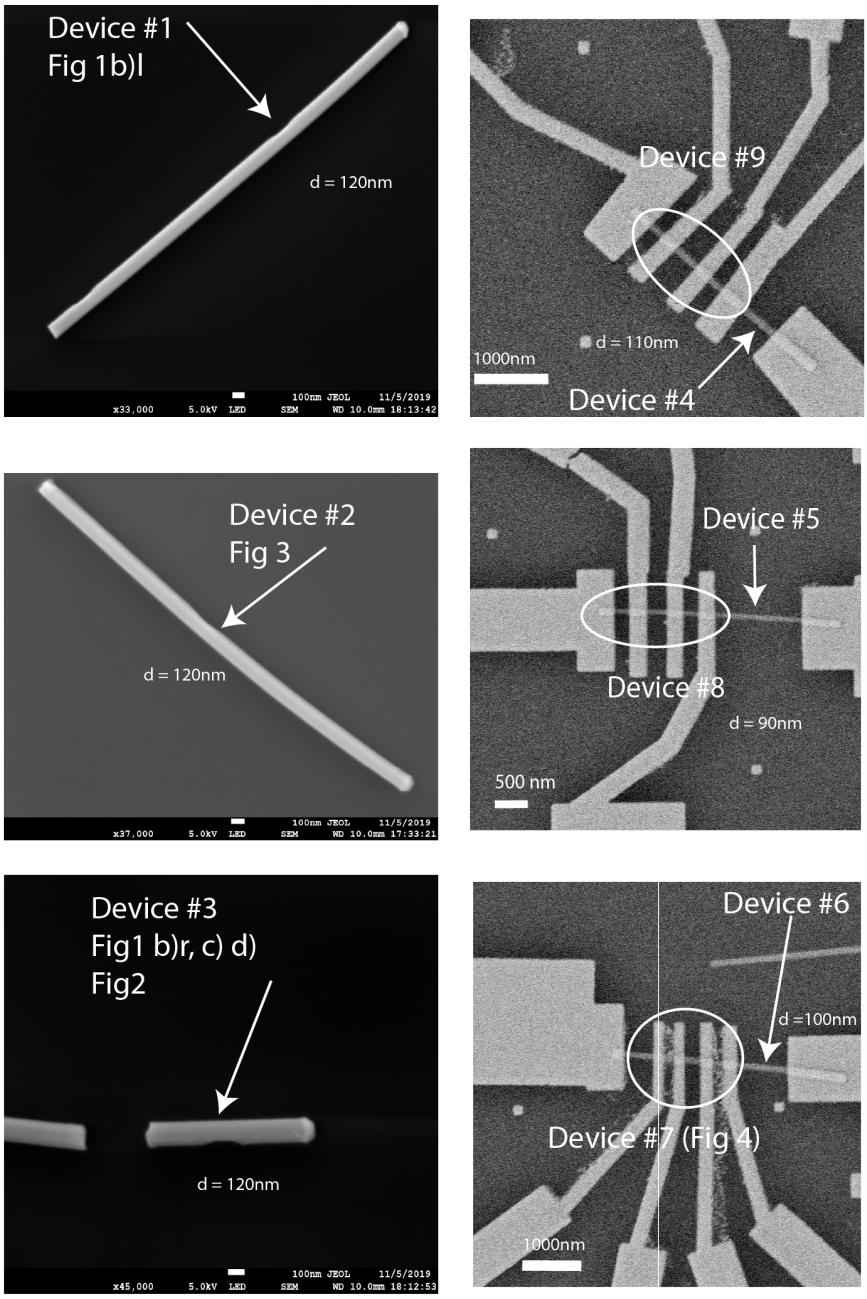

FIG. S1. This figure shows SEMs of all the devices presented in this paper. For Devices 1-3 the SEMs show the NW with the Josephson junction before contacting. An arrow highlights the position of the shadow gap. The diameter is measured from these pictures and has uncertainty ± 5nm. For Devices 4-9 the SEMs show the final device after fabrication with the ellipse showing the leads used for the four terminal junctionless measurements and arrows indicating Josephson junctions. The diameter has an uncertainty of ± 10nm. The text indicates what panels of the main text were measured on which device.

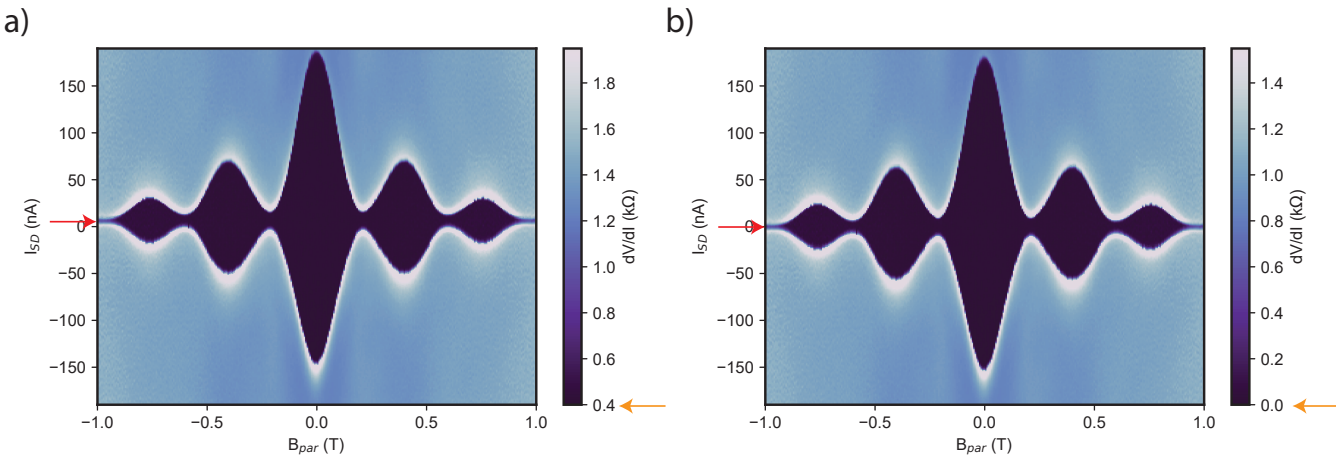

FIG. S2. This figure illustrates how the raw data of the differential resistance maps has been adjusted. a) The raw data as measured b) The corrected map. The offset of current amplifier has been detected at regions where the superconducting region becomes narrow. The center of this narrow supercurrent (red arrow) has been set to 0 nA (In this case the offset was 6.5nA). The finite contact resistance has been determined by the finite constant resistance of of the black region and was subtracted (in this case 0.4 kΩ) (orange arrow)

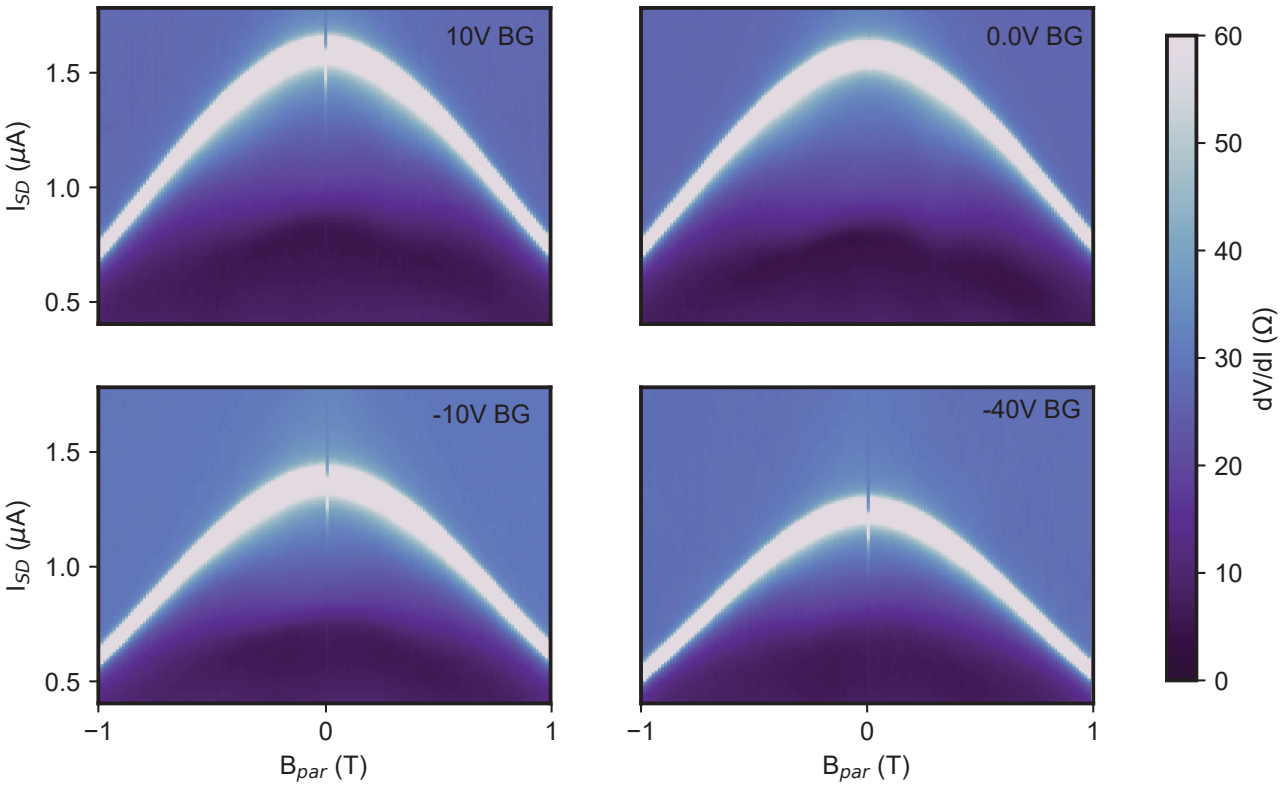

FIG. S3. This figure shows the maps which are used to extract the contours of Figure 1 d)

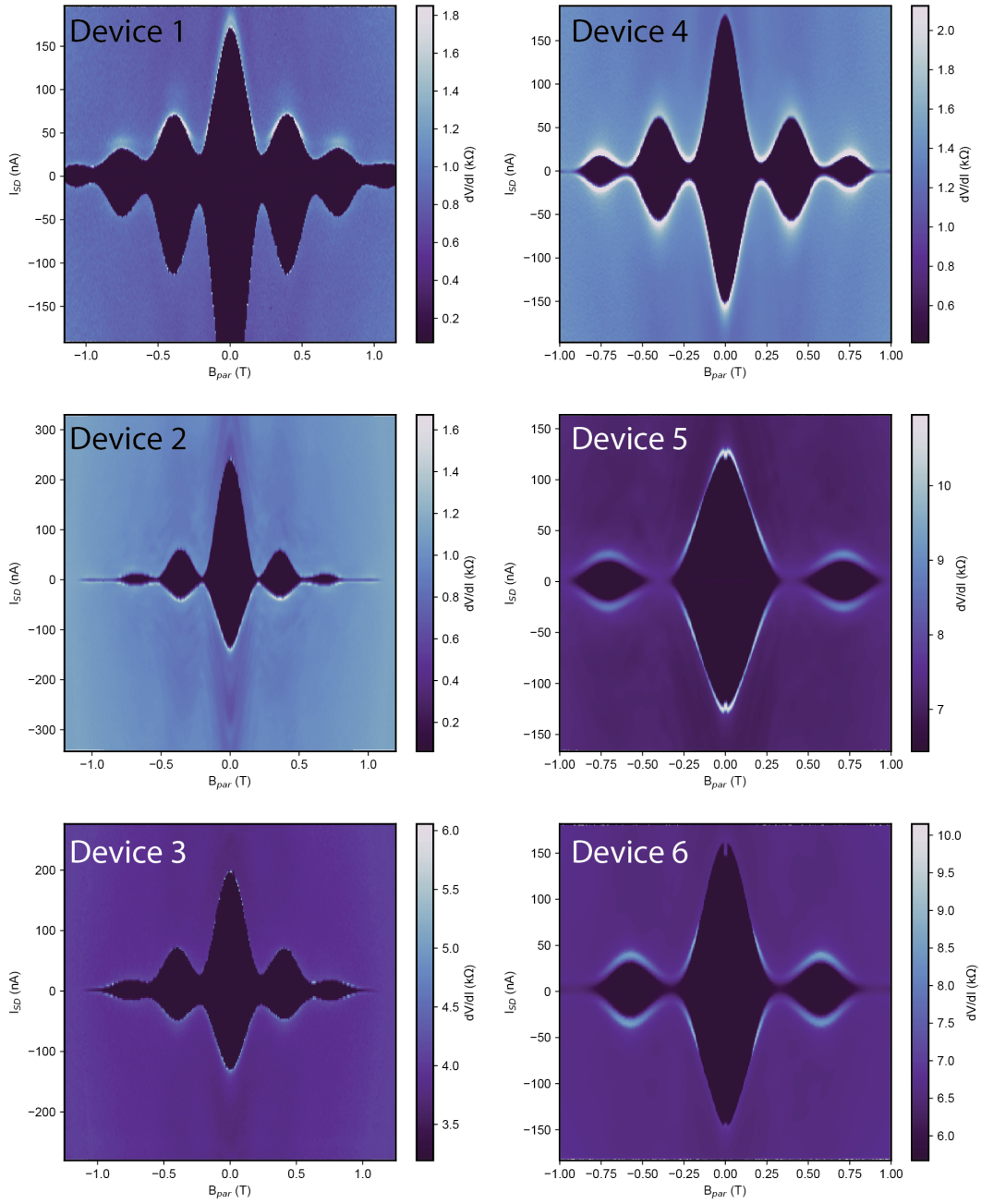

FIG. S4. This figure shows the raw data for the six Josephson junction line-traces in Figure 1 e). Those maps are taken at backgate voltage of 10V. With exception of Device 1, device are swept from lower to higher values.

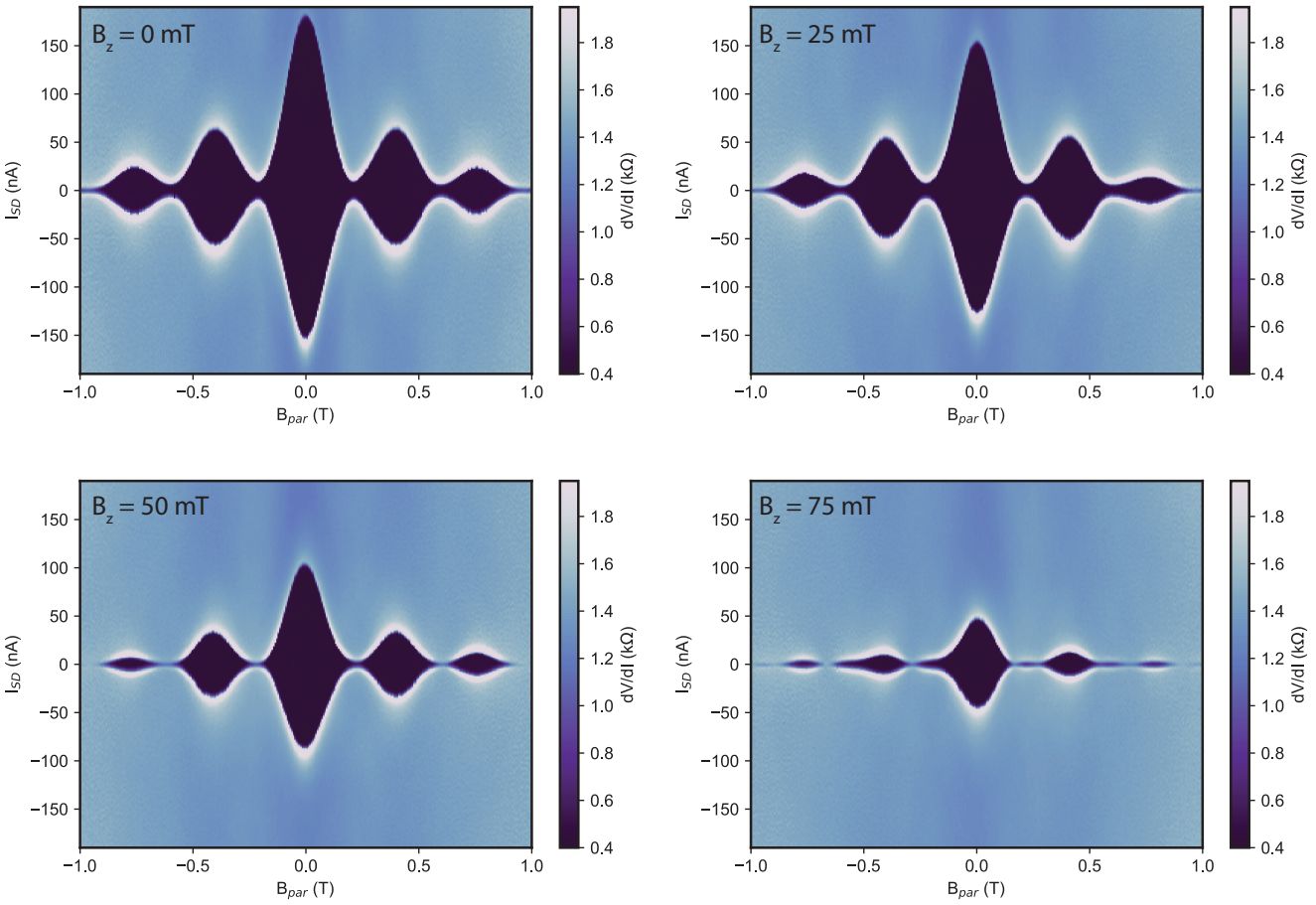

FIG. S5. This figure shows the raw data used for extracting the line-traces in Figure 2 e) from Device 3. These maps are taken at backgate voltage of 10V

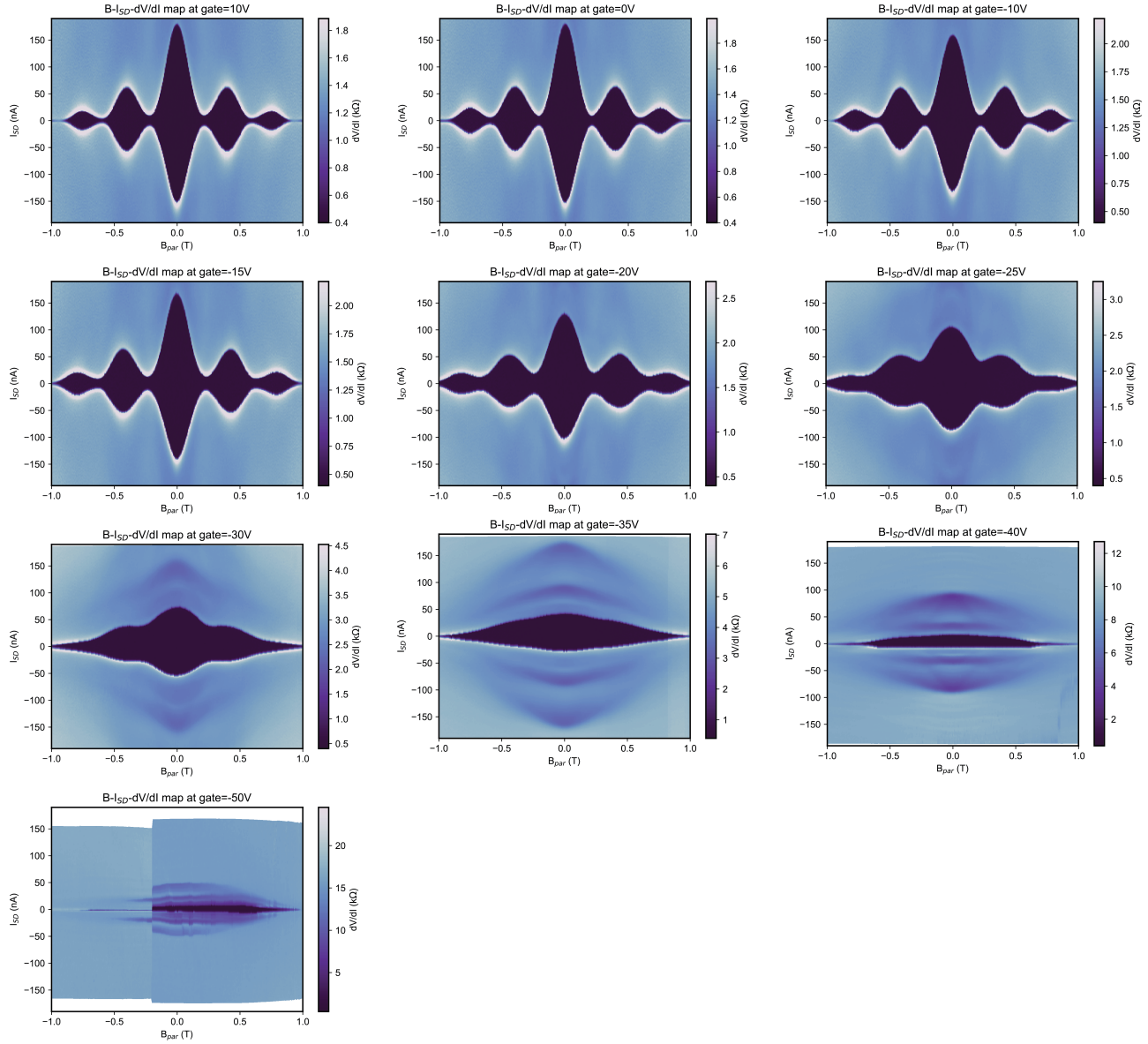

FIG. S6. This figure shows the raw data of Device 3 for extracting the line-traces in Figure 4 c). The color-scales are adjusted so the maximum is at 1.5 $R_n(V)$. The resonances outside of the critical current regions are identified as MAR. As R_n increases with more negative Gate voltages,the resonances move to lower current values. At the lowest gate values the oscillations absent for both supercurrent and for MAR features.

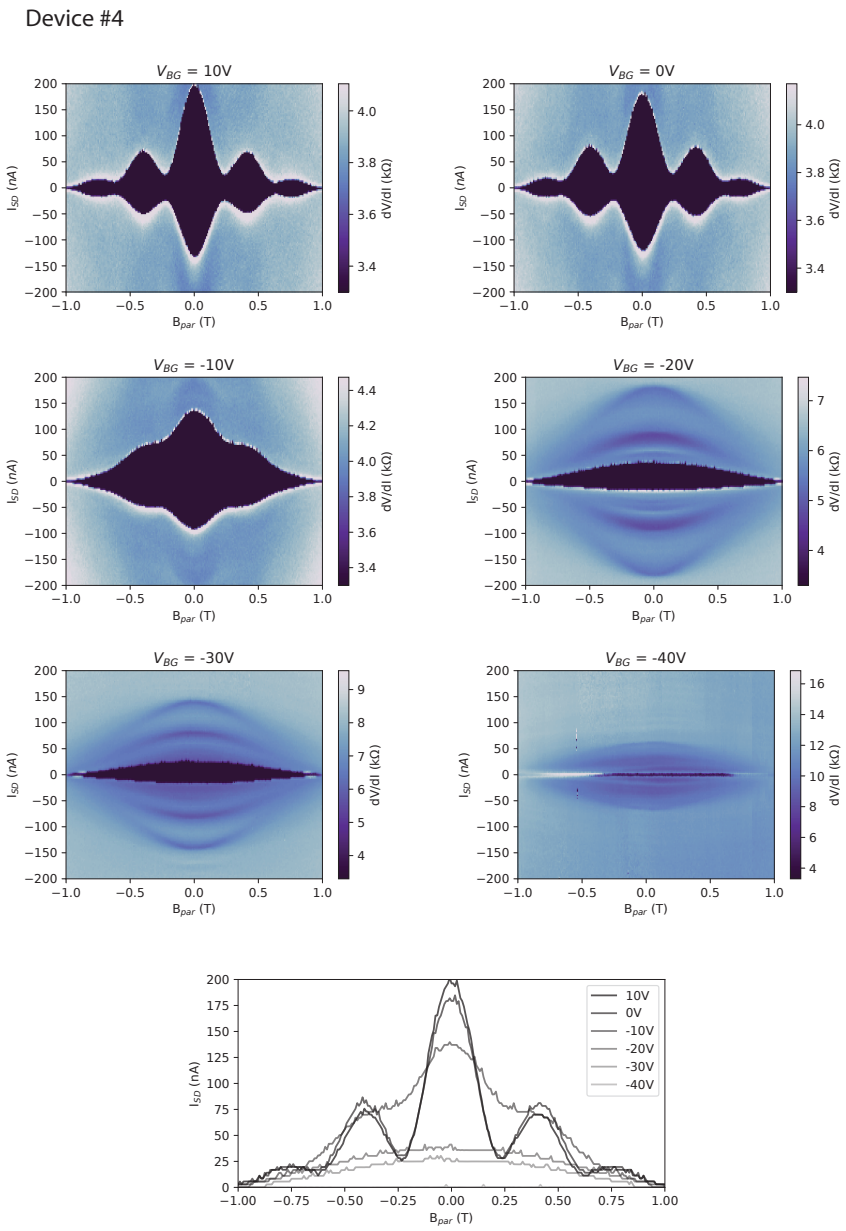

FIG. S7. This figure shows gate dependence of the super current oscillations for device 4. The color-scales are adjusted so the maxima are at 1.5 $R_n(V)$. The bottom panel shows I_{sw} extracted from the six panels above stacked, analogously to Figure 4 c) of the main text.

V_{BG}	-1st	0th	1st
10V	0.37 T	0.41 T	0.37 T
0V	0.37 T	0.4 T	0.38 T
-10V	0.38 T	0.42 T	0.39 T
-15V	0.38 T	0.45 T	0.40 T
-20V	0.43 T	0.47 T	0.42 T
-25V	0.38 T	0.47 T	0.42 T
-30V	0.39 T	0.53 T	0.37 T

TABLE I. This table shows the extracted widths of the supercurrent lobes as function of $B_{||}$ in T for Device 3 from the main text Figure 4.

* tsand@nbi.ku.dk

[1] A. Y. Kitaev, Physics-Uspekhi **44**, 131 (2001).
[2] H.-J. Kwon, K. Sengupta, and V. M. Yakovenko, The European Physical Journal B - Condensed Matter and Complex Systems **37**, 349 (2004).

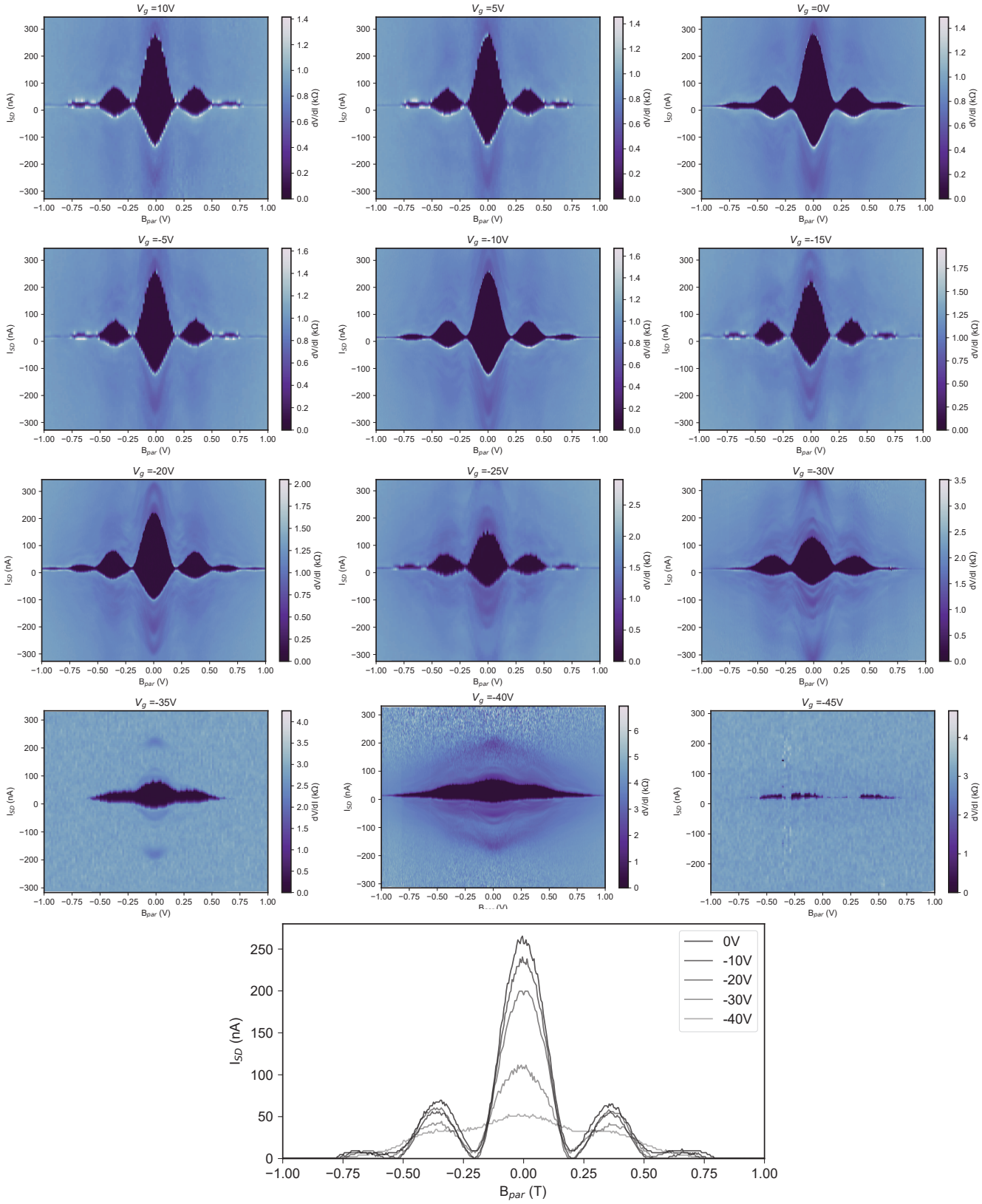

FIG. S8. This figure shows the gate dependence of the critical current oscillations for device 2. For the three lowest gate voltages the high normal state resistance R_n overloaded the voltage amplifier. This is the reason the MAR resonances are not clearly visible in these measurements. The critical current region however is visible in all gate settings, showing a similar trend to the device to S7 and Fig 4 c) in the main text. The measurements at 10 V, 5 V, -5 V, -15 V, -25 V, -35 V and -45 V were taken at fast sweep-rate and lower resolution, than the others.

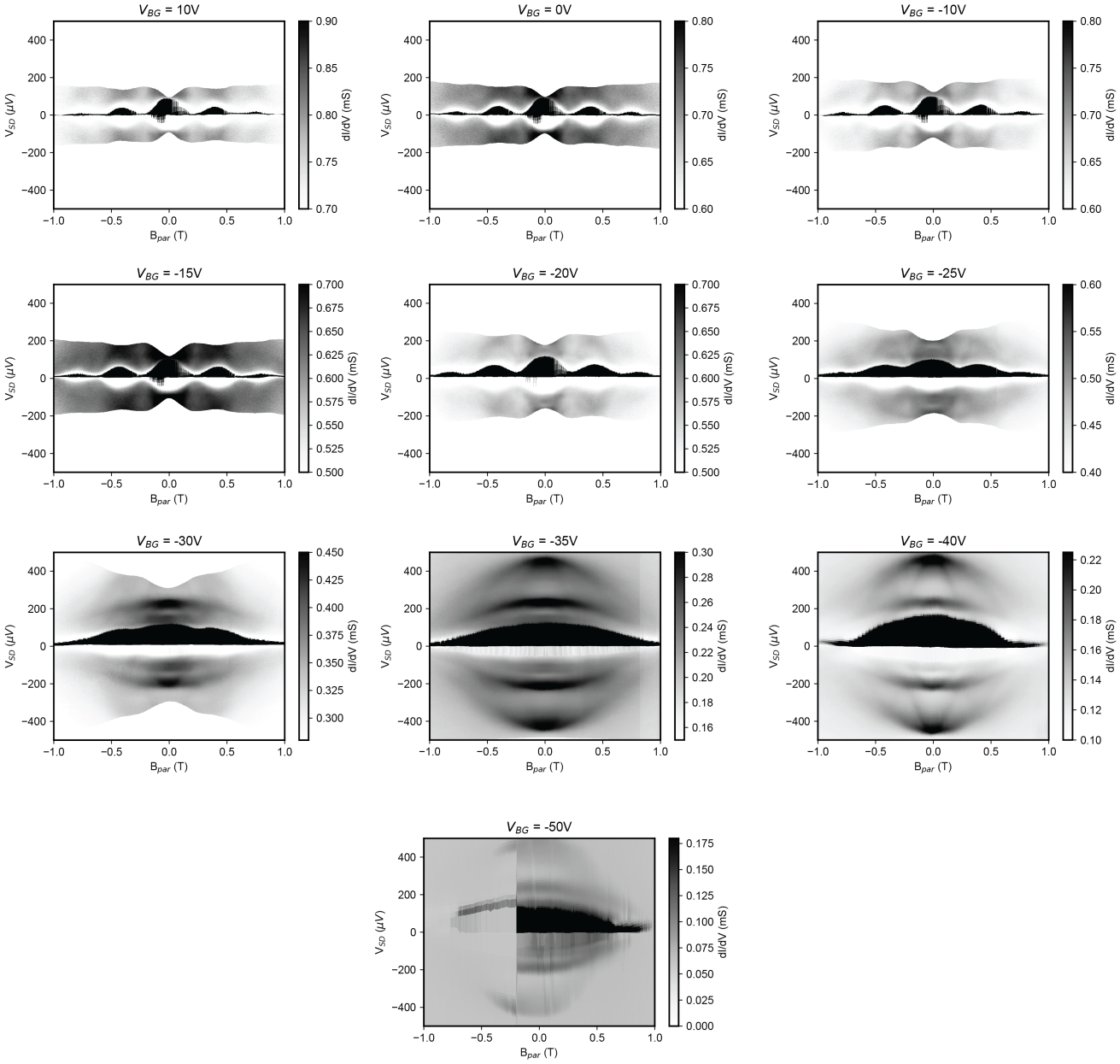

FIG. S9. This figure the same measurements as Fig S6 as differential conductance as a function of Voltage. This highlights the harmonic nature of the subgap structure. Due to the changing normal state resistance, for high gate voltages the measurement does not reach the 2Δ peak at around $440\mu V$. The qualitative behavior shows MAR peaks following the oscillating behavior of the supbercurrent down to -40V. From -35 V to -50V it is also possible to observe MAR resonance without oscillations.

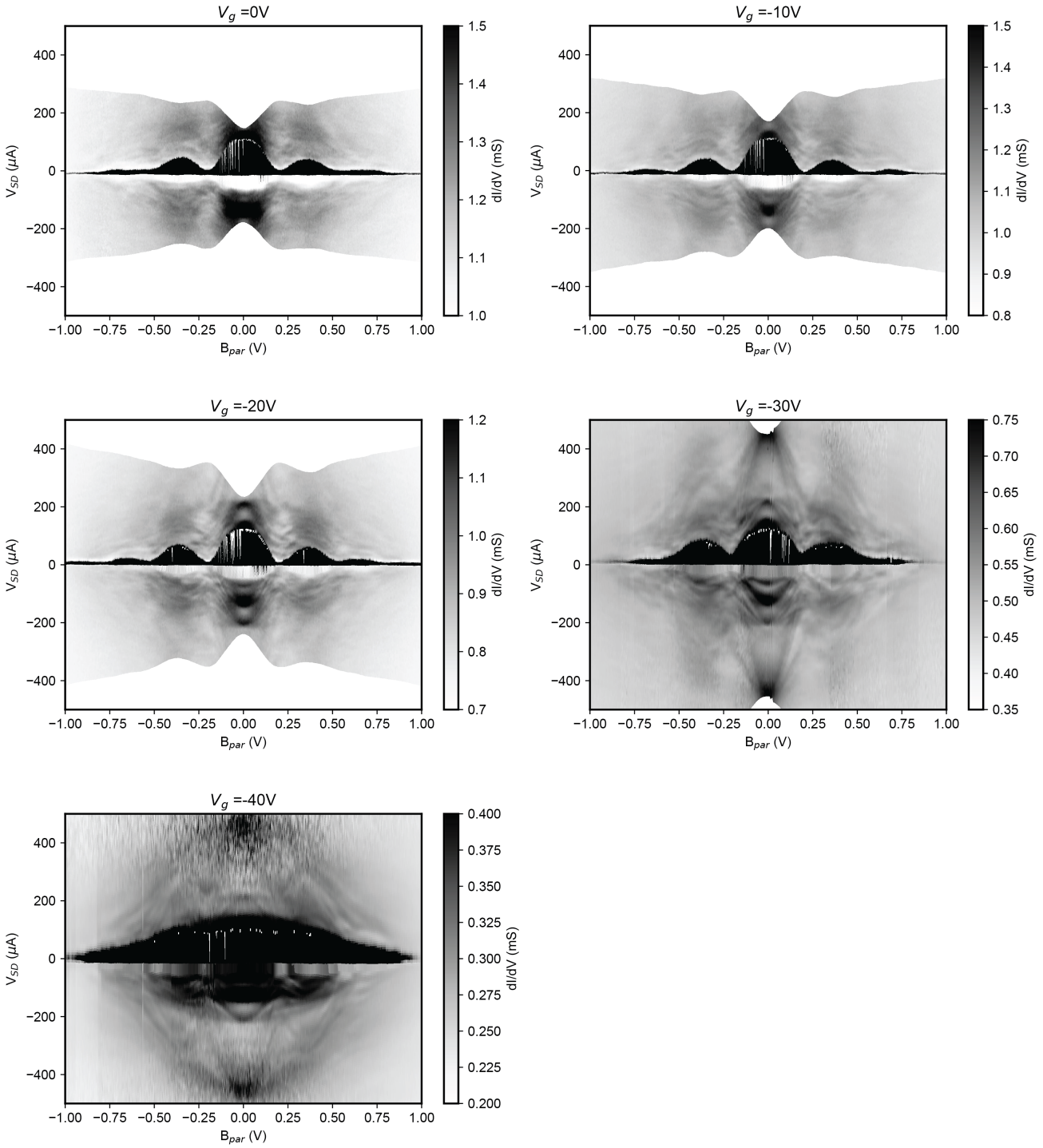

FIG. S10. This figure shows the same type of maps as Fig S9 for Device 2. The measurement for $V_{BG} = -30V$ is the same as Fig 5 c) in the main text. All measurements show the characteristic Little Parks Gap modulation

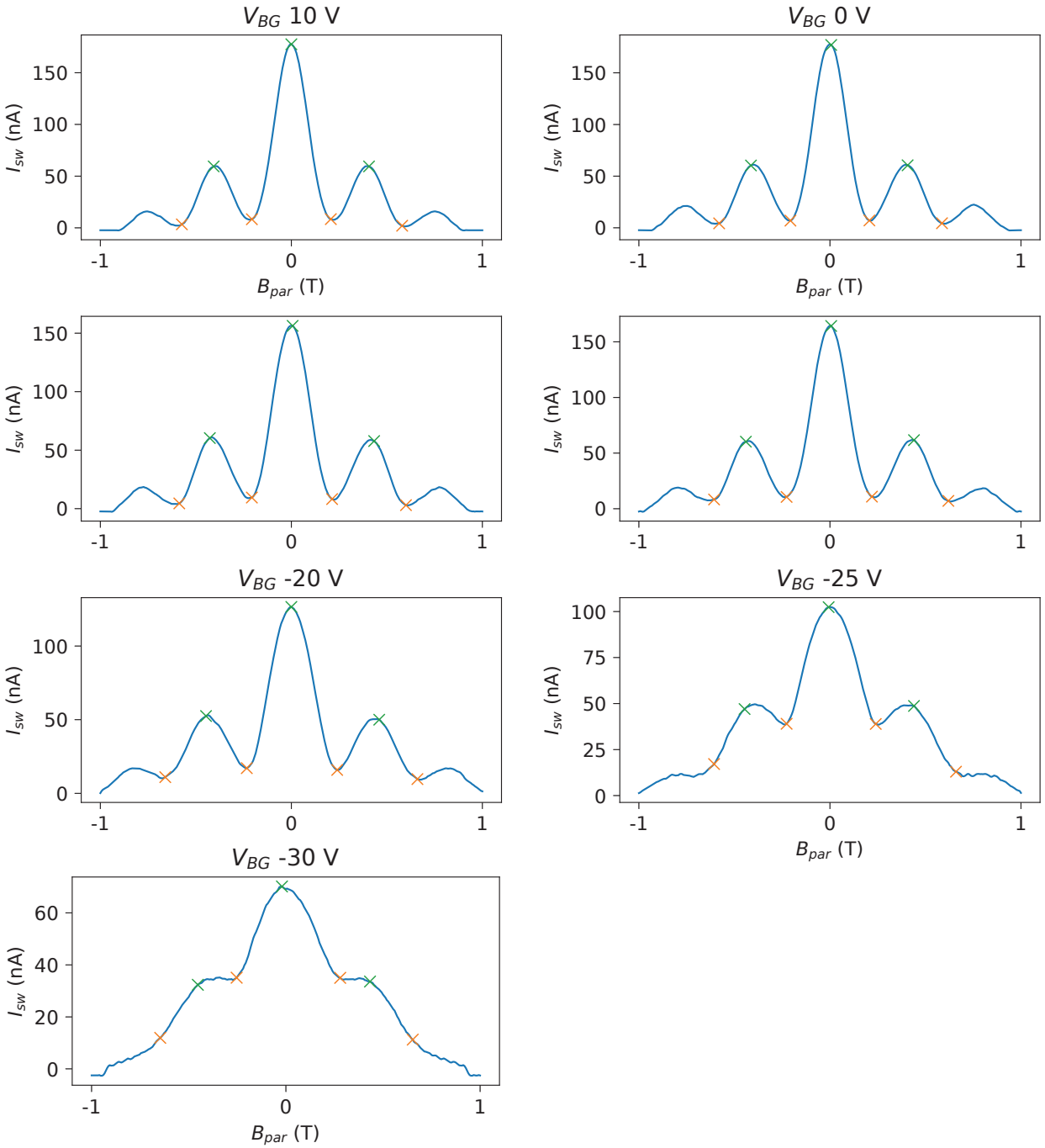

FIG. S11. This figure shows the switching current minima (orange) extracted for Table 1 in the Supporting information. The data is from Device 3. The distance between the inner two minima is what is determining ΔB in the inset of Figure 4 c)

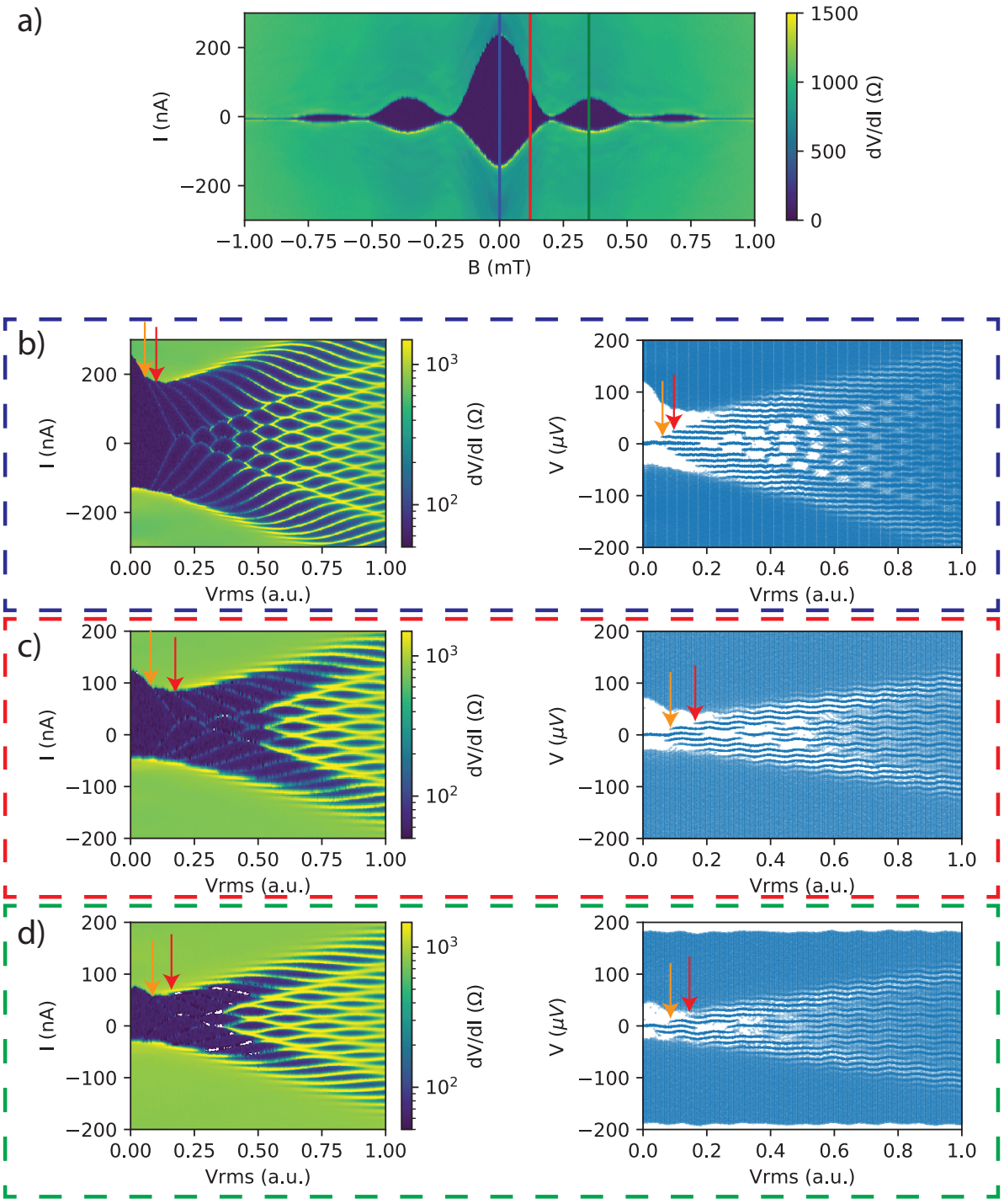

FIG. S12. This figure shows the trivial Shapiro effect we found in a the Josephson junction device 2 at $V_G = 10V$ a) Shows oscillating behavior of the critical current as a function of $B_{||}$. The lines indicate the values of $B_{||}$ at which b), c) and d) were taken. b) c) and d) Show on the left the differential resistance as a function of applied current and increasing applied RF power at a frequency of 5 GHz. We observe the typical Bessel-like widths of plateaus. The orange arrow indicates the emergence of the first Shapiro step, the red arrow the emergence of the second Shapiro step. The right panel shows the same data as a scatter plot against voltage. This highlights the quantized voltage values of Shapiro plateaus. Red and orange arrow indicate again the emergence of first and second Shapiro step. The red trace at 120 mT was chosen to roughly match the critical current of the green trace at 350 mT, this ensures potential changes of Shapiro steps are not due to changed RSJ junction dynamics. A topological Josephson junction is predicted to have 4π-periodic current phase relation [1]. A signature of such a doubling of periodicity is the doubling of the step-height of such Shapiro steps [2]. If the junction hosts both a topological and a trivial supercurrents, both voltage step amplitudes are present however at given conditions (RCSJ- and frequency parameters) the 2n-th step will appear before the (2n-1)th step. We did not observe any such behavior through a large parameter space of V_{BG} and frequency. In conclusion no topological Josephson effect with a 4π periodic dispersion was observed.

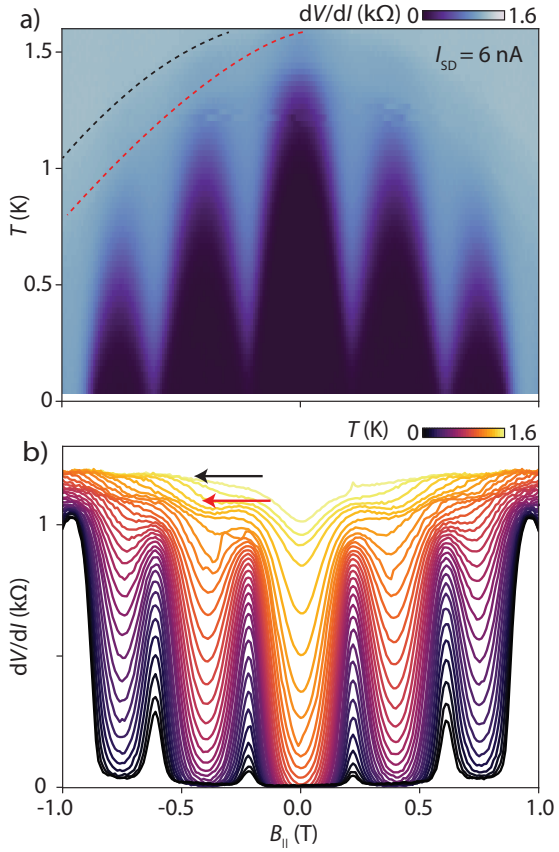

FIG. S13. (a) Differential resistance for Device 3 as a function of T and $B_{||}$ at $V_{BG} = 10$ and $I_{SD} = 6\,\mathrm{nA}$ showing the dome-shaped modulation of the critical temperature. The red and green line indicate two distinct transitions more clearly distinguished in panel (b) which shows every other row of (a) as line cuts.